JACS
JOURNAL OF THE AMERICAN CHEMICAL SOCIETY

pubs.acs.org/JACS

Communication

Water-Triggered, Irreversible Conformational Change of SARS-CoV-2 Main Protease on Passing from the Solid State to Aqueous Solution

Narjes Ansari,[‡] Valerio Rizzi,[‡] Paolo Carloni, and Michele Parrinello*

Cite This: *J. Am. Chem. Soc.* 2021, 143, 12930−12934

Read Online

ACCESS | Metrics & More | Article Recommendations | Supporting Information

ABSTRACT: The main protease from SARS-CoV-2 is a homodimer. Yet, a recent 0.1-ms-long molecular dynamics simulation performed by D. E. Shaw's research group shows that it readily undergoes a symmetry-breaking event on passing from the solid state to aqueous solution. As a result, the subunits present distinct conformations of the binding pocket. By analyzing this long simulation, we uncover a previously unrecognized role of water molecules in triggering the transition. Interestingly, each subunit presents a different collection of long-lived water molecules. Enhanced sampling simulations performed here, along with machine learning approaches, further establish that the transition to the asymmetric state is essentially irreversible.

The appearance of a new coronavirus has triggered a pandemic that is still spreading throughout the world.[1,2] The virus is closely related to other coronaviruses[3] such as SARS-CoV and MERS-CoV and has been named SARS-CoV-2. A number of vaccines were developed at an unprecedentedly fast rate and have been provided to a significant fraction of the human population.[4] However, the emergence of new variants of the virus makes it imperative to concurrently advance drug discovery.[5]

A target against SARS-CoV-2 infection is the main protease (SC-2 M^{pro} hereafter)[6−12] that cleaves the nascent viral polypeptide chain. This enzyme is a homodimer, and the presence of the two subunits is required for its biological function.[12] Each of the subunits is formed by three domains: domains I (residues 10−99) and II (residues 100−182) have an antiparallel β-barrel structure, while domain III (residues 198−303) forms a compact α-helical domain connected to domain II by a long linker loop[10] (Figure 1a,b). The enzymatic reaction is performed by the catalytic His41-Cys145 dyad, located in the S2 site of each of the subunits (see Figure S-1 in the Supporting Information (SI)).[13,14]

Although most X-ray studies on SC-2 M^{pro} show an almost perfect symmetry of the homodimer,[7] indirect evidence suggests that only one of the two subunits is catalytically active in each of the subunits, as in a variety of other homodimeric proteins.[15] (i) In the almost identical homodimeric protein from SARS-CoV (SC M^{pro}, 96% sequence identity with SC-2 M^{pro}),[7] one subunit is inactive because of distortions of the active site;[16−19] molecular dynamics (MD) provided insight on this asymmetry,[18] similarly to what has been done for other homodimeric proteins.[20,21] (ii) Different analyses of a 0.1-ms-long MD simulation, recently performed by D. E. Shaw's research group (DESRES),[22] of SC-2 M^{pro} in aqueous solution suggested that each of the two subunits visits a different set of configurations[23−25] after starting from a symmetric X-ray structure (PDB 6Y84[26]). This hints at a role of packing forces in the conformation of the protein.[27] Consistently, other MD studies suggested that only one subunit is catalytically active.[28,29]

Here we re-analyze the DESRES simulation,[22] focusing on the factors that lead to symmetry breaking. The key role of water is clearly apparent from the very first part of the trajectory, in which the initial symmetry is broken. In fact, we observe a single water molecule entering the binding pocket of one of the subunits, which starts a series of changes that lead to the disruption of the catalytic site and to symmetry breaking. As in the SC M^{pro} dimerization and (in)activation,[17] a key step is the contact breaking between the N-finger terminus (residues 1−7, Figure 1b) of one subunit and the m-shaped loop (residues 135−146, Figure 1b) of the other one. After this initial phase, a long-lived asymmetric state emerges, in which the binding pockets of the two subunits have different volumes and contain a different number of water molecules (see SI).

Could the protein swap from one asymmetric conformation to the other? Our analysis helps us in identifying a slow mode of the system that expresses the subunit active−inactive transition. By amplifying its fluctuations by means of a newly developed enhanced sampling method,[30] we are able to induce transformations in which the subunits exchange their roles. However, our estimate of the corresponding kinetic barrier is so high that on the biological time scales this event is unattainable. This reported stability of the homodimer asymmetric state is practically irreversible.

We start by illustrating how the initial symmetric configuration (PDB 6Y84[26]) shown in Figure 1a−c is broken

Received: May 23, 2021
Published: August 16, 2021

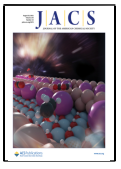

https://doi.org/10.1021/jacs.1c05301
J. Am. Chem. Soc. 2021, 143, 12930−12934

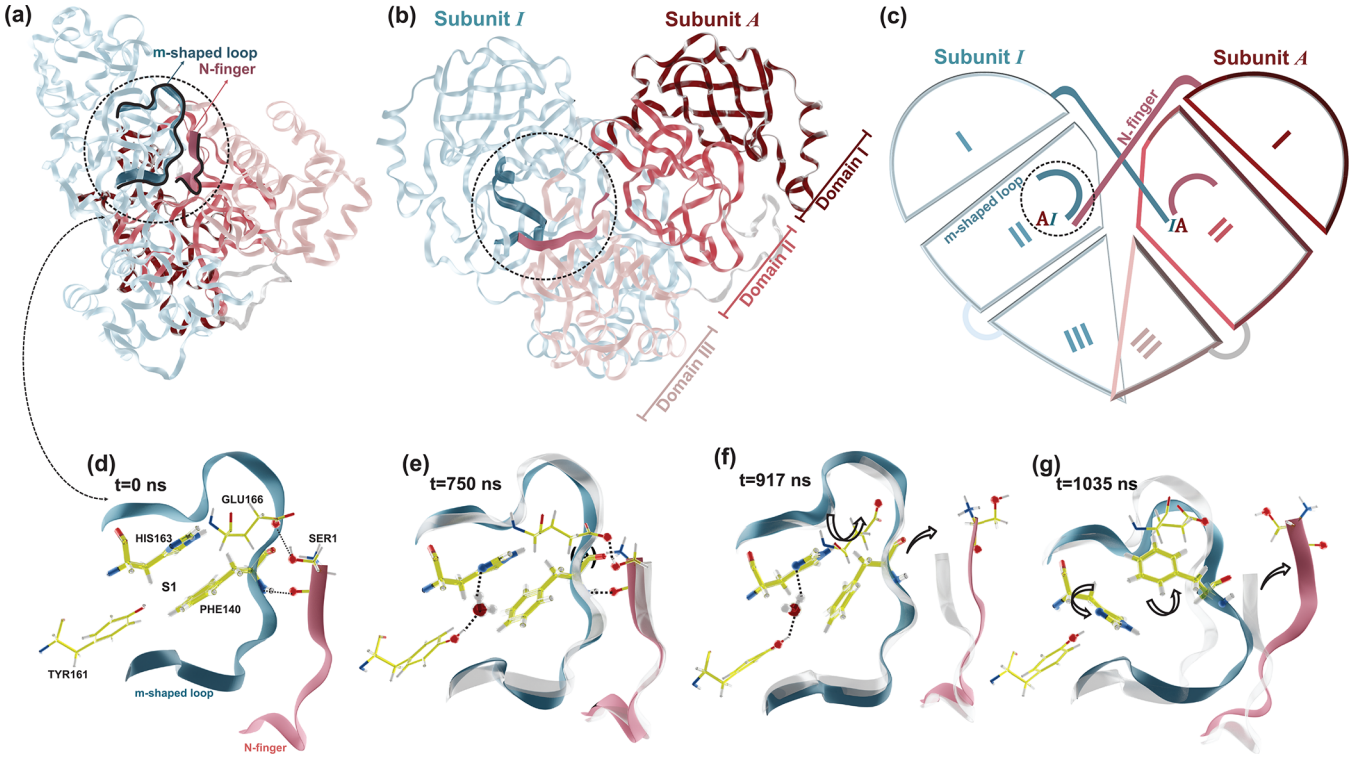

Figure 1. (a, b) Cartoons representing the SC-2 M^{pro} X-ray structure[26] from two different viewpoints. The subunits, ***I*** in light blue and ***A*** in red, consist of domains I–III. The m-shaped loop of ***I*** and the N-finger of ***A*** are shown in darker colors in a dashed circle. (c) Schematic of the protein as shown in (b). (d–g) Symmetry breaking of ***I***, as observed in the DESRES simulation.[22] This event occurs between 0.75 and 1.035 μs. Only residues relevant to the process are shown. (d) The initial conformations of the m-shaped loop and the N-finger (also in (a) and (b)). The two regions interact via the Glu166@***I***– and Phe140@***I***–Ser1@***A*** H-bonds. (e) One water enters the S1 binding pocket and forms a bridge between His163@***I*** and Tyr161@***I***. (f) A rotation of Glu166@***I*** leads to a breakage of its H-bond with the N-finger. (g) A water molecule that leaves the S1 binding pocket triggers a disruption of the hydrophobic contact between residues His163@***I*** and Phe140@***I***, leading to the deactivation of ***I***.

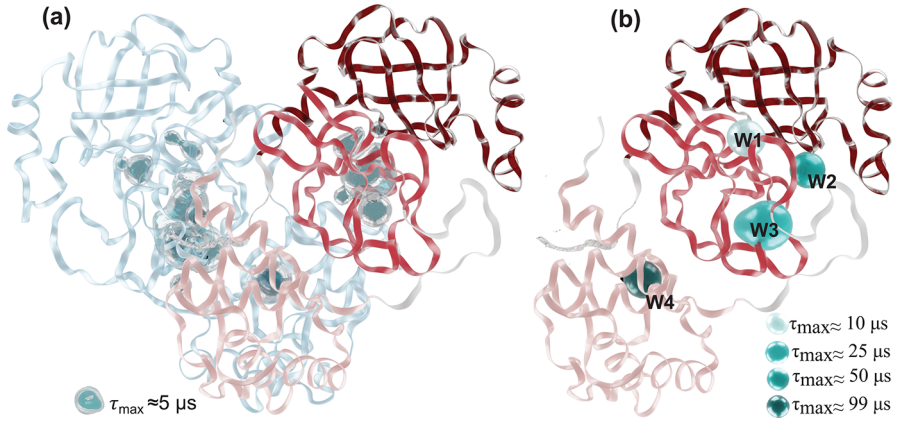

Figure 2. Average positions of (a) medium- and (b) long-lived water molecules inside of the two subunits of an SC-2 M^{pro} after 60.2 μs. In (a), the distribution of water is asymmetric and delocalized, while in (b), the distribution is symmetrical in both subunits and consists of four hydration sites (W1–W4). The water maximum lifetime τ_{max} is indicated.

in the DESRES simulation.[22] We follow in particular the intra- and inter-subunit contacts which have been shown to be crucial for the stabilization of the S1 binding pocket in SC-2 M^{pro}. Such contacts are the Phe140/His163 intra-subunit hydrophobic interaction and the inter-subunit interaction between the m-shaped loop and the N-finger, in particular the Glu166/Ser1 H-bond (Figure 1d). We name the two subunits ***A*** and ***I***, anticipating that eventually the first one will remain active and the other one will become inactive. Following the observations from ref 16, the active form, in contrast to the inactive one, satisfies simultaneously two criteria which are essential in stabilizing the S1 binding pocket (Figure 1d). First, it shows an intra-subunit π-stacking contact between side chains Phe140 and His163 (Figure 1d). Second, it has an inter-subunit hydrogen bond between its Glu166 residue and the Ser1 residue of the other subunit (Figure 1d).

After 750 ns, a water molecule bridges the imidazole nitrogen atom of His163@***I*** and the hydroxyl oxygen atom of Tyr161@***I*** (see Figure 1e). In another 150 ns, Glu166@***I*** rotates and the N-finger@***A*** changes its conformation,

https://doi.org/10.1021/jacs.1c05301
J. Am. Chem. Soc. 2021, 143, 12930–12934

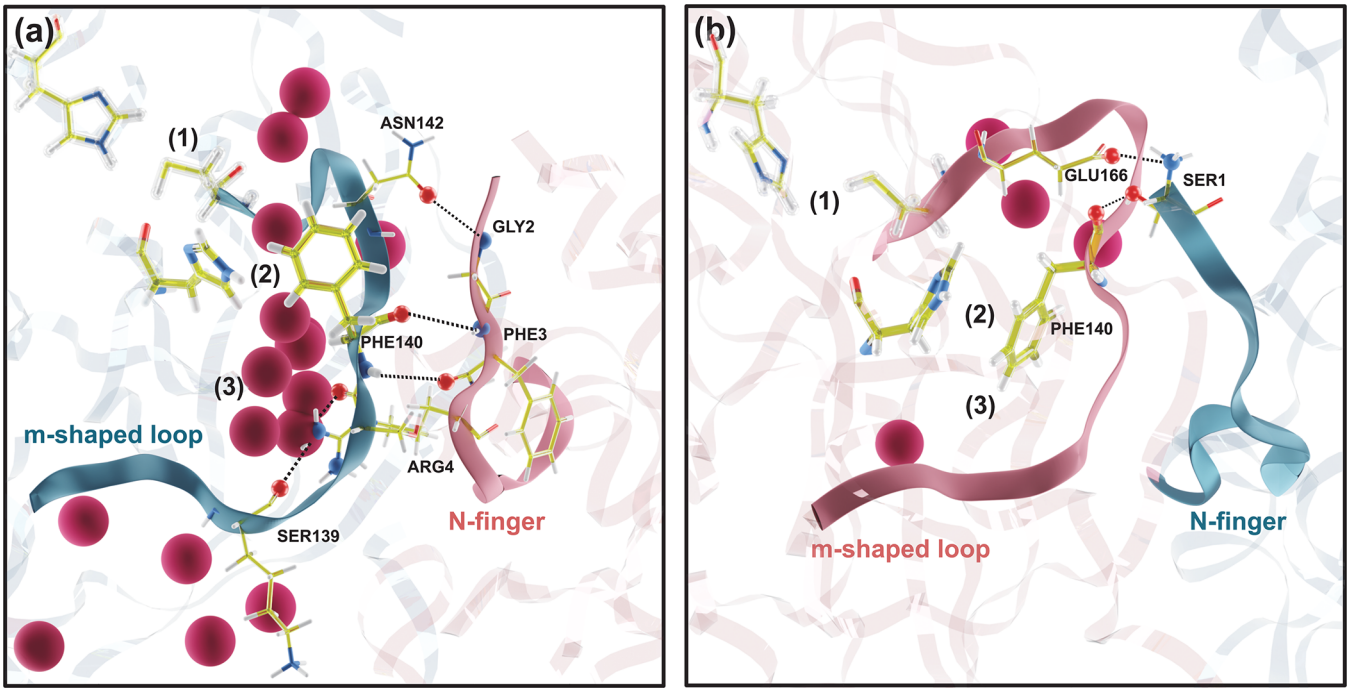

Figure 3. Conformations of the m-shaped loop and the N-finger in (a) the inactive ***I*** and (b) the active ***A*** subunits in an equilibrated structure of the DESRES simulation after 60.2 μs. The positions of hydration sites with a water occupancy larger than 50% of the time are shown as red spheres. The position of the catalytic dyad and the stackings between Phe140 and His163 and the S1 binding pocket are shown with labels (1)−(3), respectively. Relevant hydrogen bond interactions between the two subunits are highlighted by a dashed line.

disrupting the link with the m-shaped loop@***I*** (see Figure 1f). Eventually, the water molecule exits from the S1 binding pocket, leaving behind an empty space that leaves no steric hindrance to stop the rotation of residue His163@***I*** away from Phe140@***I***. The rotation breaks the catalytic dyad of ***I*** (see Figure 1g), while the one in ***A*** remains stable. This symmetry-broken state is maintained for the rest of the simulation (about 99 μs).

We concluded that water (within the well-known force field limitations[31,32]) does play a role in the disruption of one of the catalytic sites. This prompted us to investigate water dynamics. We divided the water molecules inside the subunit in two groups according to their lifetime during the last 99 μs.

The *long-lived water molecules* (with a lifetime larger than 5 μs) are located in four spots (W1−W4) whose position is symmetrical in the two subunits (Figure 2b). The lifetime increases on passing from W1 to W4. W1 and W2 bridge domains I and II, while W3 and W4 sit in domains II and III, respectively. In W4, water is deeply buried and stays for the entire dynamics. If a water molecule leaves W1−W4, it is quickly replaced by another one, supporting the notion that water in these spots may have a structural role. The water molecules lying on the W2−W4 spots are in close proximity to positions observed by X-ray crystallography, with low values of the Debye−Waller factor (PDB 6Y84,[26] see Table S-1 and Figure S-3 in the SI).

The *medium-lived water molecules* (with a lifetime between 0.5 and 5 μs) sit in non-symmetry-related positions (see Figure 2a), thus contributing to the asymmetry of what appears to be the equilibrium state. They occupy a region that encompasses the S1 binding pocket (see Figure 3). We refer to this region as the water reservoir (see SI) and to the positions where water accumulates as hydration sites. The asymmetry between subunits ***I*** and ***A*** is mirrored in the larger number of hydration sites in ***I***. Furthermore, in ***A***, the water reservoir cavity is essentially rigid and has a rather constant water occupation, while in ***I*** it exhibits volume fluctuations correlated with its content of water molecules (see SI).

The way in which the two subunits interact and their respective conformation is correlated with their medium-lived water content. In ***I***, the m-shaped loop strongly interacts with the N-finger of ***A*** via several hydrogen bonds; see Figure 3a. As a result of these interactions, the large aromatic ring of Phe140@***I*** flips (Figure 3a). This event opens up a path for water molecules to enter and, together with the reorientation of the m-shaped loop and the hydrophobic π-stacking of His163@***I*** and Phe140@***I***, leads to the collapse of the S1 binding site (indicated by label (3) in Figure 3a).

On the other hand, in ***A***, the interaction between the m-shaped loop@***A*** and the N-finger@***I*** is different (see Figure 3b). The Ser1@***I*** amino forms a hydrogen bond with the carbonyl oxygen of Glu166@***A*** and, together with the hydrophobic interaction between the His163@***A*** and Phe140@***A***, stabilizes the catalytic site (see label (3) of Figure 3b).

To determine whether the symmetry breaking can be reversed, one can use enhanced sampling simulations.[33] Here, we apply the recently developed on-the-fly probability enhanced sampling (OPES) method[30] that is the latest evolution of Metadynamics.[34,35] Just like other enhanced sampling methods, OPES requires the identification of appropriate collective variables (CVs) whose fluctuations are enhanced in a statistical mechanics compliant way.[33]

Here, the CV construction is facilitated by the insight gained by our examination of the DESRES trajectory. Our procedure requires two steps. At first, we identify 26 descriptors that are able to distinguish whether the catalytic site is active or inactive by focusing on the region in the vicinity of the m-shaped loop,

https://doi.org/10.1021/jacs.1c05301
J. Am. Chem. Soc. 2021, 143, 12930−12934

the N-finger, and the S1 binding pocket (see SI). Albeit these descriptors focus on the protein conformation, we were guided in their choice by the location of the hydration sites; thus, water indirectly takes part in the descriptor set.

As a second step, we apply Deep-LDA,[36,37] a machine-learning-based procedure that, given a set of descriptors and their fluctuations, is able to generate efficient CVs in the study of transitions between metastable states. In our case, the states in question are the configurations of the active and the inactive subunits from the DESRES trajectory. By applying the resulting CV independently to both subunits and starting from the symmetry-broken homodimer state, we facilitate transitions to the flipped homodimer where the two subunits exchange their role. The ability of the CV to trigger transitions crucially reflects the insight gained from our previous analysis.

We run a number of exploratory OPES simulations where, in about 100 ns, we observe a few forth and back subunit exchange events (see SI) that occur smoothly without passing via unnatural conformations, reflecting the use of meaningful CVs (see movie in the SI). Calculating an accurate free energy surface is beyond present-day capabilities, given the size and complexity of the system. However, we found it of interest to determine, even if in an approximate form, the free energy barrier corresponding to the subunit flip (see SI).

We estimate the barrier to lie between 125 and 150 kJ/mol, which corresponds to an extremely rare event at room temperature. Of course, such an estimate must be taken with a lot more than a grain of salt. Nevertheless, considering that the transition's characteristic time far exceeds the SC-2 M^{pro} lifetime, we can be reasonably confident to say that the SC-2 M^{pro} asymmetric homodimer state is indeed irreversible.

In conclusion, our analysis of the long simulation in ref 22 on SC-2 M^{pro}, complemented by enhanced sampling simulations, suggests that water molecules in one of the two subunits trigger a transition from a symmetric to an asymmetric state in which only one of the two subunits is functional. Such a transition is irreversible.

■ ASSOCIATED CONTENT

Supporting Information

The Supporting Information is available free of charge at https://pubs.acs.org/doi/10.1021/jacs.1c05301.

Details on the DESRES trajectory analysis with a focus on the role played by water, details on the enhanced sampling simulations, Tables S-1 and S-2, and Figures S-1−S-9 (PDF)

Movie showing forth and back subunit exchange event (MP4)

■ AUTHOR INFORMATION

Corresponding Author

Michele Parrinello − *Italian Institute of Technology, 16152 Genova, Italy*; Email: michele.parrinello@iit.it

Authors

Narjes Ansari − *Italian Institute of Technology, 16152 Genova, Italy*; orcid.org/0000-0003-2017-8431

Valerio Rizzi − *Italian Institute of Technology, 16152 Genova, Italy*; orcid.org/0000-0001-5126-8996

Paolo Carloni − *Computational Biomedicine, Institute for Advanced Simulation (IAS-5) and Institute of Neuroscience and Medicine (INM-9), and JARA-Institute "Molecular Neuroscience and Neuroimaging" (INM-11), Forschungszentrum Jülich, Jülich 52425, Germany; Physics Department, RWTH Aachen University, Aachen 52074, Germany*; orcid.org/0000-0002-9010-0149

Complete contact information is available at: https://pubs.acs.org/10.1021/jacs.1c05301

Author Contributions

‡N.A. and V.R. contributed equally to this paper.

Notes

The authors declare no competing financial interest.

■ ACKNOWLEDGMENTS

We acknowledge the Italian Institute of Technology (IIT) for funding and support. The simulations were performed on the supercomputer CLAIX-2016-GPU at Forschungszentrum Jülich. The project was supported by the Helmholtz European Partnering program between Jülich and IIT. Part of this work was performed under the auspices of ETH Zürich and Università della Svizzera Italiana, Lugano. We thank David Shaw's group for making their long MD trajectory available to the scientific community. We also thank Giulia Rossetti for reading the manuscript and giving us useful suggestions.

■ REFERENCES

(1) Wu, F.; et al. A new coronavirus associated with human respiratory disease in China. *Nature* **2020**, *579*, 265−269.

(2) Zhou, P.; et al. A pneumonia outbreak associated with a new coronavirus of probable bat origin. *Nature* **2020**, *579*, 270−273.

(3) Masters, P. S. *Adv. Virus Res.* **2006**, *66*, 193−292.

(4) Kyriakidis, N. C.; López-Cortés, A.; González, E. V.; Grimaldos, A. B.; Prado, E. O. SARS-CoV-2 vaccines strategies: a comprehensive review of phase 3 candidates. *npj Vaccines* **2021**, *6*, 28.

(5) Dolgin, E. The race for antiviral drugs to beat COVID — and the next pandemic. *Nature* **2021**, *592*, 340−343.

(6) Jin, Z.; et al. Structure of Mpro from SARS-CoV-2 and discovery of its inhibitors. *Nature* **2020**, *582*, 289−293.

(7) Zhang, L.; Lin, D.; Sun, X.; Curth, U.; Drosten, C.; Sauerhering, L.; Becker, S.; Rox, K.; Hilgenfeld, R. Crystal structure of SARS-CoV-2 main protease provides a basis for design of improved α-ketoamide inhibitors. *Science* **2020**, *368*, 409−412.

(8) Ullrich, S.; Nitsche, C. The SARS-CoV-2 main protease as drug target. *Bioorg. Med. Chem. Lett.* **2020**, *30*, 127377.

(9) Joshi, R. S.; Jagdale, S. S.; Bansode, S. B.; Shankar, S. S.; Tellis, M. B.; et al. Discovery of potential multi-target-directed ligands by targeting host-specific SARS-CoV-2 structurally conserved main protease. *J. Biomol. Struct. Dyn.* **2021**, *39*, 3099−3114.

(10) Lee, J.; Worrall, L. J.; Vuckovic, M.; Rosell, F. I.; Gentile, F.; Ton, A.-t.; Caveney, N. A.; Ban, F.; Cherkasov, A.; Paetzel, M.; Strynadka, N. C. J. Crystallographic structure of wild-type SARS-CoV-2 main protease acyl-enzyme intermediate with physiological C-terminal autoprocessing site. *Nat. Commun.* **2020**, *11*, 5877.

(11) Kneller, D. W.; Phillips, G.; O'Neill, H. M.; Jedrzejczak, R.; Stols, L.; Langan, P.; Joachimiak, A.; Coates, L.; Kovalevsky, A. Structural plasticity of SARS-CoV-2 3CL Mpro active site cavity revealed by room temperature X-ray crystallography. *Nat. Commun.* **2020**, *11*, 3202.

(12) El-Baba, T. J.; Lutomski, C. A.; Kantsadi, A. L.; Malla, T. R.; John, T.; Mikhailov, V.; Bolla, J. R.; Schofield, C. J.; Zitzmann, N.; Vakonakis, I.; Robinson, C. V. Allosteric Inhibition of the SARS-CoV-2 Main Protease: Insights from Mass Spectrometry Based Assays**. *Angew. Chem., Int. Ed.* **2020**, *59*, 23544−23548.

(13) Świderek, K.; Moliner, V. Revealing the molecular mechanisms of proteolysis of SARS-CoV-2 M pro by QM/MM computational methods. *Chemical Science* **2020**, *11*, 10626−10630.

(14) Ramos-Guzmán, C. A.; Ruiz-Pernía, J. J.; Tuñón, I. Unraveling the SARS-CoV-2 Main Protease Mechanism Using Multiscale Methods. *ACS Catal.* **2020**, *10*, 12544−12554.
(15) Brown, J. H. Breaking symmetry in protein dimers: Designs and functions. *Protein Sci.* **2006**, *15*, 1−13.
(16) Yang, H.; Yang, M.; Ding, Y.; Liu, Y.; Lou, Z.; Zhou, Z.; Sun, L.; Mo, L.; Ye, S.; Pang, H.; Gao, G. F.; Anand, K.; Bartlam, M.; Hilgenfeld, R.; Rao, Z. The crystal structures of severe acute respiratory syndrome virus main protease and its complex with an inhibitor. *Proc. Natl. Acad. Sci. U. S. A.* **2003**, *100*, 13190−13195.
(17) Shi, J.; Sivaraman, J.; Song, J. Mechanism for Controlling the Dimer-Monomer Switch and Coupling Dimerization to Catalysis of the Severe Acute Respiratory Syndrome Coronavirus 3C-Like Protease. *J. Virol.* **2008**, *82*, 4620−4629.
(18) Chen, H.; Wei, P.; Huang, C.; Tan, L.; Liu, Y.; Lai, L. Only One Protomer Is Active in the Dimer of SARS 3C-like Proteinase. *J. Biol. Chem.* **2006**, *281*, 13894−13898.
(19) Xia, B.; Kang, X. Activation and maturation of SARS-CoV main protease. *Protein Cell* **2011**, *2*, 282−290.
(20) Salsbury, F. R.; Yuan, Y.; Knaggs, M. H.; Poole, L. B.; Fetrow, J. S. Structural and Electrostatic Asymmetry at the Active Site in Typical and Atypical Peroxiredoxin Dimers. *J. Phys. Chem. B* **2012**, *116*, 6832−6843.
(21) Na, I.; Catena, D.; Kong, M.; Ferreira, G.; Uversky, V. Anti-Correlation between the Dynamics of the Active Site Loop and C-Terminal Tail in Relation to the Homodimer Asymmetry of the Mouse Erythroid 5-Aminolevulinate Synthase. *Int. J. Mol. Sci.* **2018**, *19*, 1899.
(22) D. E. Shaw Research. *Molecular Dynamics Simulations Related to SARS-CoV-2, D. E. Shaw Research Technical Data*, 2020; http://www.deshawresearch.com/resources_sarscov2.html (accessed Dec 1, 2020).
(23) Carli, M.; Sormani, G.; Rodriguez, A.; Laio, A. Candidate Binding Sites for Allosteric Inhibition of the SARS-CoV-2 Main Protease from the Analysis of Large-Scale Molecular Dynamics Simulations. *J. Phys. Chem. Lett.* **2021**, *12*, 65−72.
(24) Cocina, F.; Vitalis, A.; Caflisch, A. Sapphire-Based Clustering. *J. Chem. Theory Comput.* **2020**, *16*, 6383−6396.
(25) Gossen, J.; et al. A Blueprint for High Affinity SARS-CoV-2 Mpro Inhibitors from Activity-Based Compound Library Screening Guided by Analysis of Protein Dynamics. *ACS Pharmacology & Translational Science* **2021**, *4*, 1079−1095.
(26) Owen, C.; et al. *RCSB PDB - 6Y84: SARS-CoV-2 main protease with unliganded active site (2019-nCoV, coronavirus disease 2019, COVID-19)*, 2020; https://www.rcsb.org/structure/6Y84 (accessed Dec 1, 2020).
(27) Godoy-Ruiz, R.; Krejcirikova, A.; Gallagher, D. T.; Tugarinov, V. Solution NMR Evidence for Symmetry in Functionally or Crystallographically Asymmetric Homodimers. *J. Am. Chem. Soc.* **2011**, *133*, 19578−19581.
(28) Verma, N.; Henderson, J. A.; Shen, J. Proton-Coupled Conformational Activation of SARS Coronavirus Main Proteases and Opportunity for Designing Small-Molecule Broad-Spectrum Targeted Covalent Inhibitors. *J. Am. Chem. Soc.* **2020**, *142*, 21883−21890.
(29) Jaffrelot Inizan, T.; Célerse, F.; Adjoua, O.; El Ahdab, D.; Jolly, L.-H.; Liu, C.; Ren, P.; Montes, M.; Lagarde, N.; Lagardère, L.; Monmarché, P.; Piquemal, J.-P. High-resolution mining of the SARS-CoV-2 main protease conformational space: supercomputer-driven unsupervised adaptive sampling. *Chemical Science* **2021**, *12*, 4889−4907.
(30) Invernizzi, M.; Parrinello, M. Rethinking Metadynamics: From Bias Potentials to Probability Distributions. *J. Phys. Chem. Lett.* **2020**, *11*, 2731−2736.
(31) Bellissent-Funel, M.-C.; Hassanali, A.; Havenith, M.; Henchman, R.; Pohl, P.; Sterpone, F.; van der Spoel, D.; Xu, Y.; Garcia, A. E. Water Determines the Structure and Dynamics of Proteins. *Chem. Rev.* **2016**, *116*, 7673−7697.
(32) Piana, S.; Donchev, A. G.; Robustelli, P.; Shaw, D. E. Water dispersion interactions strongly influence simulated structural properties of disordered protein states. *J. Phys. Chem. B* **2015**, *119*, 5113−5123.
(33) Valsson, O.; Tiwary, P.; Parrinello, M. Enhancing Important Fluctuations: Rare Events and Metadynamics from a Conceptual Viewpoint. *Annu. Rev. Phys. Chem.* **2016**, *67*, 159−184.
(34) Laio, A.; Parrinello, M. Escaping free-energy minima. *Proc. Natl. Acad. Sci. U. S. A.* **2002**, *99*, 12562−12566.
(35) Barducci, A.; Bussi, G.; Parrinello, M. Well-Tempered Metadynamics: A Smoothly Converging and Tunable Free-Energy Method. *Phys. Rev. Lett.* **2008**, *100*, 020603.
(36) Bonati, L.; Rizzi, V.; Parrinello, M. Data-Driven Collective Variables for Enhanced Sampling. *J. Phys. Chem. Lett.* **2020**, *11*, 2998−3004.
(37) Rizzi, V.; Bonati, L.; Ansari, N.; Parrinello, M. The role of water in host-guest interaction. *Nat. Commun.* **2021**, *12*, 93.

https://doi.org/10.1021/jacs.1c05301
J. Am. Chem. Soc. 2021, 143, 12930−12934